

Magnetospheric Scattering and Emission in Millisecond Pulsars

Timothy M. Braje and Roger W. Romani

Department of Physics, Stanford University, Stanford, CA 94035

timb@astro.stanford.edu; rwr@astro.stanford.edu

ABSTRACT

We model the formation of magnetospheric components of millisecond pulsar light curves, deriving an approximate model for the curved space, ‘swept-back’ dipole field and following photon emission, propagation, and scattering. Magnetospheric pulse components are strongly affected by rapid rotation and Schwarzschild effects.

Subject headings: stars:neutron—pulsars:general—magnetic fields

1. Introduction and Light Curve Model

With the launch of *CXO* and *XMM-Newton*, there has been a dramatic increase in sensitivity for high resolution X-ray studies of compact objects. Rapidly rotating neutron stars are targets of particular interest, since measurements of the stellar surface can probe the neutron star evolution and the equation of state at high density. Several relativistic effects may also be visible, in some cases. A number of millisecond pulsars (MSP) have been observed in the X-rays, both as isolated rotation powered objects (Becker & Triumper 1999) and as accretion powered LMXBs (e.g. Wijndands & van der Klis 1998). In Braje, Romani, & Rauch (2000), we explored the distortions of the surface emission imparted by rapid rotation, including the important effects of Doppler boosting, aberration, and gravitational focusing and time delays. More subtle effects induced by frame dragging were also considered. For rotation-powered pulsars, the surface radiation must traverse the magnetosphere, where resonant scattering can introduce significant distortions in the pulse profile (Rajagopal & Romani 1997). Further, several X-ray MSP have narrow, non-thermal pulse components, suggesting a direct origin in the magnetosphere. In this paper, we extend the treatment of rapid rotation effects to include scattering and emission in a surrounding dipole magnetosphere.

Our model assumes a spherical star, which we take to be sufficiently centrally condensed that

a Schwarzschild (or Kerr) metric is an adequate model of the external spacetime (the ‘Roche approximation’). Because we wish to extend the modeling to small spin periods P_* , the effects of ‘sweep-back’ on the magnetic field, even for r a few times the stellar mass M , can be substantial. In addition, the rapid rotation develops large electro-motive forces. We follow the common assumption that this EMF causes pair production such that the closed zone of the magnetosphere is filled with a charge-separated pair plasma, whose charge distribution cancels the rotational EMF. For the magnetic field, we assume a point dipole located at the stellar center and generalize the computation of the field structure for the non-rotating dipole in the Schwarzschild spacetime (e.g., Bardeen & Press 1973; Prasanna & Gupta 1997; Muslimov & Harding 1997). Our result passes smoothly to the Schwarzschild magnetic field \mathbf{B} as the stellar angular velocity Ω_* vanishes and to the flat space rotating dipole solution as $r \rightarrow \infty$. We assume that the plasma co-rotates (is stationary) in the closed zone, which is defined by the ‘last closed’ field lines traced from tangent approach to the light cylinder at $r_{LC} = c P_*/2\pi$ to the stellar surface.

Our light curve modeling follows the procedure described in Braje et al. (2000). This Monte Carlo code starts with photons randomly drawn from the surface emission zone, with initial directions drawn from a model limb-darkened distribution. We aberrate these surface photons and

propagate to infinity through curved space, using the Schwarzschild or Kerr metric, as appropriate. As the photon passes through the magnetosphere, we monitor for local cyclotron resonance. At the resonance position photons are re-emitted with the proper boosted scattering angular distribution. We also follow photons arising directly from the magnetosphere — from acceleration gaps or other non-thermal sources. After including the gravitational and time-of-flight delays, the photons are assigned to energy and rotational phase bins to produce maps of the radiation on the sky. Slices through these maps at the Earth's viewing angle provide pulsar light curves and phase-resolved spectra.

2. Magnetic Field Structure

We have developed an approximate, retarded, dipolar magnetic field expression that links the exact non-rotating Schwarzschild result at small r with the flat space ‘swept-back’ field structure at large r . We expect the magnetic field lines to have approximately the same shape as a static dipole near the star, but to curve back near the light cylinder, as Figure 1 displays.

To derive our magnetic field expression, we write Maxwell’s Stress Tensor as derivatives of the vector potential in covariant form as

$$F_{\mu\nu} = \frac{\partial A_\nu}{\partial x^\mu} - \frac{\partial A_\mu}{\partial x^\nu}. \quad (1)$$

We use the Schwarzschild metric in geometrized units ($G = c = 1$):

$$ds^2 = \eta^2 dt^2 - \frac{dr^2}{\eta^2} - r^2 d\theta^2 - r^2 \sin^2 \theta d\phi^2 \quad (2)$$

where $\eta = \sqrt{1 - 2M/r}$. If we solve Maxwell’s Equations in vacuum

$$F^{\mu\nu}_{;\mu} = 0 \quad (3)$$

for a dipole moment $\mu = \mu \hat{z}$ we arrive at the solution in the Schwarzschild spacetime

$$A_\phi(r, \theta) = f(r) \frac{\mu \sin^2 \theta}{r} \quad (4)$$

where we have written the expression as the flat-space result weighted by the multiplicative function:

$$f(r) = \frac{3r^3}{8M^3} \left[\log \eta^2 + \frac{2M}{r} \left(1 + \frac{M}{r} \right) \right] \quad (5)$$

(e.g., Wasserman & Shapiro 1983). For the more general rotating case, we multiply the flat space time dependent vector potential by the same function $f(r)$:

$$\mathbf{A} = f(r) \left\{ \frac{\boldsymbol{\mu}(t) \times \mathbf{r}}{r^3} + \frac{\dot{\boldsymbol{\mu}}(t) \times \mathbf{r}}{r^2} \right\} \quad (6)$$

where we now have a time dependent dipole moment, $\boldsymbol{\mu}(t) = \mu(-\sin \alpha \cos \Omega_*(t-r), -\sin \alpha \sin \Omega_*(t-r), \cos \alpha)$, tilted with respect to the rotational (z) axis by an angle α . We use $\{\mathbf{e}_t, \mathbf{e}_r, \mathbf{e}_\theta, \mathbf{e}_\phi\}$ to denote the coordinate basis vectors and $\{\mathbf{e}_\hat{t}, \mathbf{e}_\hat{r}, \mathbf{e}_\theta, \mathbf{e}_\phi\}$ for the orthonormal basis vectors. By taking the dot product of the vector potential with the coordinate basis vectors, we obtain the vector potential components $(A_t, A_r, A_\theta, A_\phi)$. Using

$$\begin{aligned} B_{\hat{r}} &= F_{\hat{\phi}\hat{r}} &= \frac{1}{r^2 \sin \theta} F_{\phi\theta} \\ B_{\hat{\theta}} &= F_{\hat{r}\hat{\theta}} &= \frac{\eta}{r \sin \theta} F_{r\phi} \\ B_{\hat{\phi}} &= F_{\hat{\theta}\hat{r}} &= \frac{\eta}{r} F_{\theta r} \end{aligned} \quad (7)$$

(c.f. Muslimov & Harding 1997) and the definition of Maxwell’s Stress Tensor (eqn. 1), we derive an expression for the field:

$$\begin{aligned} B_{\hat{r}} &= \frac{6\mu}{(2M)^3} \chi \left[-\cos \alpha \cos \theta \right. \\ &\quad \left. + \sin \alpha \sin \theta \left(\cos \tilde{\phi} + r\Omega_* \sin \tilde{\phi} \right) \right] \\ B_{\hat{\theta}} &= \frac{3\mu\eta}{(2M)^3} \left[r^2 \Omega_*^2 \chi \cos \theta \cos \tilde{\phi} \sin \alpha \right. \\ &\quad \left. + 2 \left(\log \eta^2 + \frac{x(1-x/2)}{\eta^2} \right) \{ \cos \alpha \sin \theta \right. \\ &\quad \left. + \cos \theta \sin \alpha \left(\cos \tilde{\phi} + r\Omega_* \sin \tilde{\phi} \right) \} \right] \\ B_{\hat{\phi}} &= \frac{3\mu\eta \sin \alpha}{(2M)^3} \left[-r^2 \Omega_*^2 \chi \sin \tilde{\phi} \right. \\ &\quad \left. + \left(\frac{x(2-x)}{\eta^2} + 2 \log \eta^2 \right) \left(r\Omega_* \cos \tilde{\phi} - \sin \tilde{\phi} \right) \right] \end{aligned} \quad (8)$$

with $x = 2M/r$, $\chi = \log \eta^2 + x(1 + x/2)$, and $\tilde{\phi} = \phi - \Omega_*(t-r)$.

The above expressions recover the familiar results in the appropriate limits: for $M \rightarrow 0$ we obtain the flat space retarded fields and for $\Omega_* \rightarrow 0$ we get the Schwarzschild expression for a dipole tilted with an angle α with respect to the z axis. Checking Maxwell’s Equations (3), we find that two are exactly satisfied ($\nu = 1, 4$). The other two are nonzero with leading terms of order $\mathcal{O}[(\Omega_* r/c)^2 (GM/rc^2)]$.

In Figure 1, we display the field line differences induced at small r in curved space coordinates. We have drawn field lines from the stellar surface

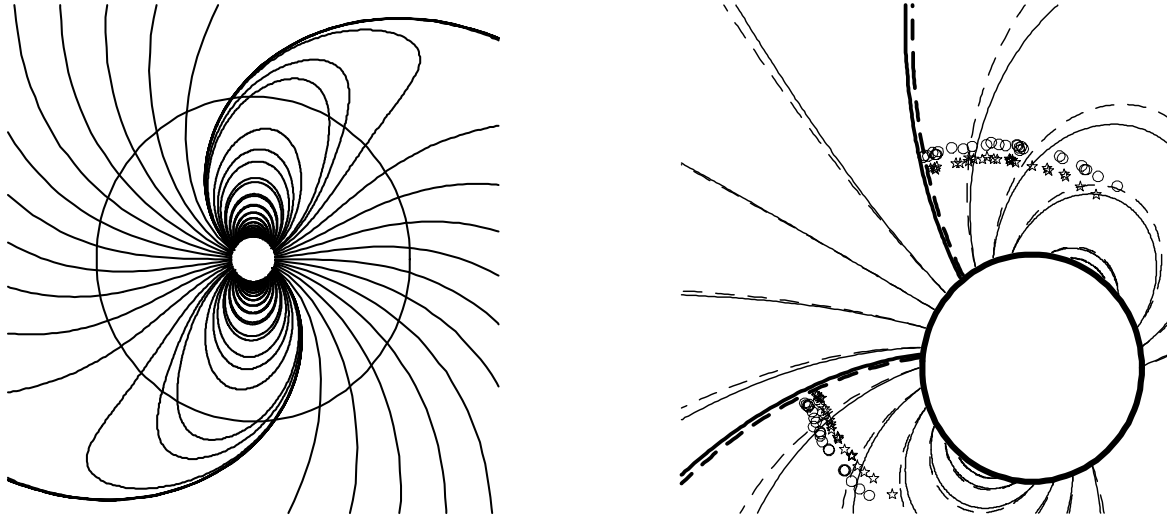


Fig. 1.— *Left Panel* – Retarded dipolar magnetic field viewed down the rotational axis. The light cylinder is depicted as a circle on top of the field lines. *Right Panel* – Curved space magnetic field perturbations viewed in the μ - Ω_* plane. Flat space (dashed lines) and curved space (solid lines) — the ‘last closed’ field lines are drawn bolder. The points show the closed zone resonant scattering locus for Schwarzschild (circles) and flat space (stars) fields, $P_* = 1.5\text{ms}$, and the same narrow range of photon energy (2.8eV–3.0eV). B is set by the same magnetic moment $\mu(r = \infty)$.

in the Ω_* - μ plane. Note that the field lines are pulled closer to the star by curved space distortions. The open field lines are nearly radial and thus display smaller curved space distortions.

3. Magnetospheric Scattering

Surface photons (*e.g.* from a thermal polar cap) must propagate through the magnetosphere surrounding the pulsar. Photons having an energy in the correct range pass through a local cyclotron resonance in the magnetosphere. For each photon energy, this defines a re-emission shell in the closed zone (Figure 1) in which strong scattering off the e^\pm re-directs flux along the local magnetic field line direction. For millisecond pulsars with $B \sim 10^8 - 10^9$ gauss, closed zone resonance typically occurs for photons of energy 1 – 10eV. With typical surface temperatures of a heated polar cap at 10^6K , this radiation falls in the Rayleigh-Jeans part of the blackbody spectrum.

In our Monte Carlo code, each photon trajectory represents a range of emitted photon energies. For each photon energy E_γ , we find the local cyclotron resonance position along the curved

space path as the photon redshifts to lower energy. For rapidly rotating stars, we must include Doppler shifts by boosting the redshifted photon energy into the local plasma rest frame, checking for resonance, re-emitting in this locally co-rotating frame, and then boosting back to the lab frame where we continue to integrate the photon trajectory. We do not scatter at open zone resonance positions, since these are assumed to have no stationary plasma.

In principle, photons can undergo multiple scatterings in the magnetosphere, for sufficiently large optical depth τ . Following Rajagopal & Romani (1997), we estimate τ assuming a stationary, flat space dipolar magnetic field. The cyclotron energy as a function of distance from the star is

$$E_c = 11.6 B_{12}^* (1 + 3 \cos^2 \theta_B)^{1/2} (R_*/r)^3 \text{keV} \quad (9)$$

where B_{12}^* is the equatorial surface dipole field strength in units of 10^{12} gauss, θ_B is the polar angle between the dipole moment and the direction of the local magnetic field, and R_* is the neutron star radius. The resonant cyclotron cross section

is

$$\sigma_{\text{res}} = \frac{\alpha_F h^2}{m_e} |e_-|^2 \delta(E_\gamma - E_c), \quad (10)$$

where e_- contains the dependence on the photon direction and polarization and α_F is the fine structure constant (e.g., Mészáros 1992). We assume a co-rotation (Goldreich-Julian) charge density $n_{\text{GJ}} = 7 \times 10^{13} B_{12}^z / P_*(\text{ms}) \text{ cm}^{-3}$ (Goldreich & Julian 1969). For rapid magnetospheric pair production the total e^\pm density may, of course, be higher. Integrating the resonant cross section through the co-rotation charge density we get the optical depth for scattering

$$\begin{aligned} \tau_{\text{GJ}}(E_\gamma) &= \int_{R_*}^{\infty} n(r) \sigma_{\text{res}} dr \\ &= \frac{2.3}{P_*(\text{ms})} B_{12}^{*1/3} \left(\frac{3\text{eV}}{E_\gamma} \right)^{1/3} \frac{B_z}{B} \frac{R_*}{10\text{km}} \end{aligned} \quad (11)$$

where we have taken $\langle |e_-|^2 \rangle = 1/3$.

For concreteness, we adopt fiducial parameters for a millisecond pulsar ($P_* = 3\text{ms}$, $R_* = 10\text{km}$, and $B_* = 10^9$ gauss); these give a characteristic optical depth of $\tau = 7.7 \times 10^{-2} B_z / B$ for $E_\gamma = 3\text{eV}$. For polar cap emission, the average optical depth is typically somewhat smaller as significant flux travels through the scattering-free open zone. Thus, for co-rotation charge densities, we neglect multiple scatterings.

In Figure 2, we plot light curves for thermal emission from a single polar cap, including closed zone scattering. The asymmetry in the scattered flux for the simple Schwarzschild propagations is due to the field ‘sweep-back’. Doppler boosts, aberration, and time delay effects are quite important, producing asymmetry in the direct flux and further phase shifting the scattered components. The ‘inter-pulse’ peaks in the scattered flux are due to radiation scattered back past the star and gravitationally focused to produce peaked pulse components. The strong energy dependence of the location of the scattering screen can be seen in the shifts of this pulse component. Note that the scattering amplitude decreases with E_γ as is apparent from equation (11). The energy dependence of the phase shifts is larger for rapid rotators (small P_*), as the high altitude scattering acquires additional aberration and Doppler boosting. Formally, these scattered radiation components provide a precision probe of the near star gravitational field, with field geometry and other systematics calibrated through the energy dependence of the component phase. In principle, precision tests of strong gravity are possible. We have run the code with Kerr metric propagations to check the detectability of these effects. At $P_* = 1.5\text{ms}$ we find frame dragging shifts the positions of the scattered photon peaks (Figure 2) by $\Delta\phi \sim 0.01$. We conclude that unless neutron stars are very compact at short periods, or unless closed zone plasmas substantially exceed the co-rotation density, frame dragging effects will be quite difficult to measure in scattered photons from surface thermal emission.

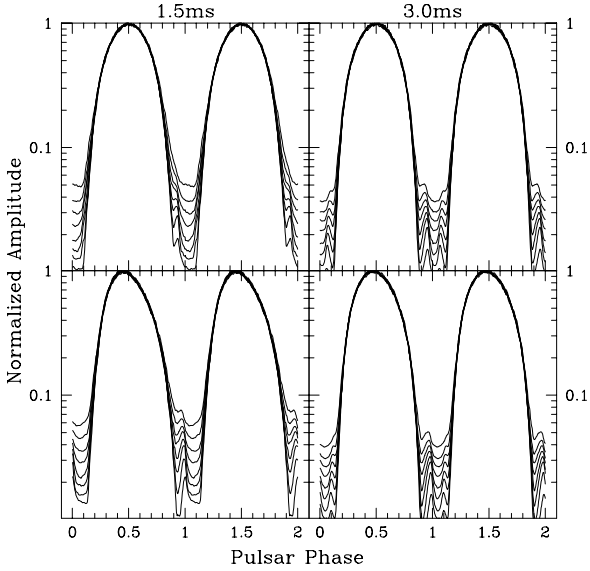


Fig. 2.— Normalized MSP light curves for a single thermal cap and viewing angle $\zeta = 115^\circ$, including closed zone resonant scattering. *Left* – $P_* = 1.5\text{ms}$. *Right* – $P_* = 3.0\text{ms}$. *Upper panels* – simple Schwarzschild metric propagations. *Lower panels* – propagations include Doppler shifts and time delays. Curves are plotted for $E_\gamma = 1.6\text{eV}$ (top) to 16eV (bottom).

tional field, with field geometry and other systematics calibrated through the energy dependence of the component phase. In principle, precision tests of strong gravity are possible. We have run the code with Kerr metric propagations to check the detectability of these effects. At $P_* = 1.5\text{ms}$ we find frame dragging shifts the positions of the scattered photon peaks (Figure 2) by $\Delta\phi \sim 0.01$. We conclude that unless neutron stars are very compact at short periods, or unless closed zone plasmas substantially exceed the co-rotation density, frame dragging effects will be quite difficult to measure in scattered photons from surface thermal emission.

4. Outer Gap Emission

As a straightforward extension of these models, we consider the effects of spacetime curvature on the light curves from outer gap emission, updating the work of Romani & Yadigaroglu (1995) to include curved space propagations. The outer

gap region follows the edge of the closed zone extending from the ‘null charge surface’ (where n_{GJ} changes sign, *i.e.* $B_z = 0$) to r_{LC} . In outer gap models this region remains charge-starved, large potential drops develop, particles accelerate, and non-thermal radiation is produced tangent to the local B (e.g., Cheng, Ho, & Ruderman 1986; Romani 1996). For MSP, this emission zone comes very close to the neutron star surface where space-time curvature becomes important.

To find the null charge boundary, we make a bicubic spline of the closed zone surface and step out along the grid until $B_z = 0$. We emit tangentially from the ‘last closed’ field line surface with an emissivity $F \propto r^{-3/2}$. As described in Romani & Yadigaroglu (1995) aberration, boosts, and time delays are all essential for any outer gap light curve computation. Accordingly, here we check the additional distortions induced by curved space effects, as might be important for millisecond pulsars.

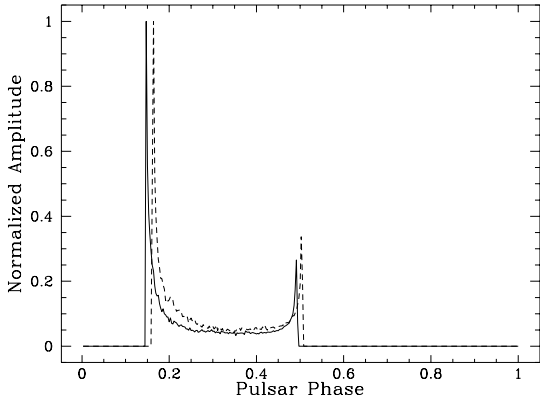


Fig. 3.— Light curves for outer gap emission. $P_* = 1.5\text{ms}$, $\alpha = 65^\circ$, $\zeta = 115^\circ$. The magnetic axis (polar cap) is at phase 0.5. Schwarzschild light curves (solid line) differ from flat space curves (dashed line) in both pulse phase and width.

In Figure 3, we show sample light curves for outer gap emission. The phase of the magnetic axis may be inferred from the structure of the radio polarization data and so the relative phasing of the high energy (outer gap) pulse is significant. Of course even classical pulsar radio emission, if arising from more than a few R_* , will show similar phase shifts, so comparison of light curve phases

must account for the altitude of the radio emission zone. The effect of neglecting Schwarzschild propagations is to both compress the pulse and shift it to later phase. For our fiducial parameters the first pulse component arises at high altitude. The second pulse arises from small r where the cap field lines (and photon directions) are nearly radial, allowing only small gravitational bending. The curved space differences are thus dominated by the phase delays induced by the retardation in the strong near surface field. The curved space pulse expansion (relative to flat space) can similarly be attributed to gravitational time delay, since the first peak arises at larger r where these effects are small.

5. Conclusions and Observational Prospects

We have improved the modeling of light curves of rapidly rotating neutron stars (MSP) by extending the description of the surrounding vacuum dipole magnetosphere to include curved space and rapid rotation effects up to corrections of order $\mathcal{O}[(\Omega_* r/c)^2(GM/rc^2)]$. These effects produce substantial changes in the pulse components introduced by magnetospheric resonant scattering (for thermal surface emission) or direct emission from the rotating magnetosphere (high altitude gap radiation). We have developed a Monte Carlo code to compute light curves illustrating these effects including the energy dependence of the scattered photon pulse shapes. Higher order effects from frame dragging have also been computed, but these are likely too subtle to be discernible in magnetospheric pulse components unless the S/N is very high. Scattering perturbations, though small, will be greatly enhanced if the magnetosphere can support a plasma with $\tau > \tau_{GJ}$. In this paper, we have only considered the minimum possible scattering perturbation. With new detector technologies (e.g. Romani et al. 1999), we should see a marked increase in the quality of optical light curves. With enhanced sensitivity and spectral resolution (and possibly higher scattering τ), light curve perturbations due to rapid rotation effects may be promoted to important probes of pulsar physics.

This work was supported in part by NASA grant NAG5-3263. Roger W. Romani is a Cottrell

Scholar of Research Corporation.

REFERENCES

Bardeen, J.M. & Press, W.H. 1973, *Journal of Mathematical Physics*, 14, 7

Becker, W. & Trümper, J. 1999, *A&A*, 341, 803

Braje, T.M., Romani, R.W., & Rauch, K.P. 2000, *ApJ*, 531, 447

Cheng, K.S., Ho, C., & Ruderman, M. 1986, *ApJ*, 300, 500

Goldreich, P. & Julian, W.H. 1969, *ApJ*, 157, 869

Mészáros, P. 1992, *High Energy Radiation from Magnetized Neutron Stars* (Chicago:University of Chicago Press)

Muslimov, A. & Harding, A. K. 1997, *ApJ*, 485, 735

Prasanna, A. R. & Gupta, A. 1997, *Nuovo Cimento B*, 112B, 1089

Rajagopal, M. & Romani, R.W. 1997, *ApJ*, 491, 296

Romani, R.W. 1996, *ApJ*, 470, 469

Romani, R.W., Miller, A.J., Cabrera, B., Figueiroa-Feliciano, E., & Nam, S.W. 1999, *ApJ*, 521, 153

Romani, R.W. & Yadigaroglu, I.-A. 1995, *ApJ*, 438, 314

Wasserman, I., & Shapiro, S. L. 1983, *ApJ*, 265, 1036

Wijnands, R., & van der Klis, M. 1998, *Nature*, 394, 344